Applied Physics A (2023) 129:499
https://doi.org/10.1007/s00339-023-06776-x

Applied Physics A
Materials Science & Processing

Study of the structural and morphological characteristics of the $Cd_xTe_yO_z$ nanocomposite obtained on the surface of the CdS/ZnO heterostructure by the SILAR method

Yana Suchikova[1] · Sergii Kovachov[1] · Ihor Bohdanov[1] · Zhakyp T. Karipbaev[2] · Vladimir Pankratov[3] · Anatoli I. Popov[3]

Received: 14 May 2023 / Accepted: 11 June 2023 / Published online: 21 June 2023

Abstract
$Cd_xTe_yO_z$ nanocomposite films were grown by the SILAR method on the CdS/ZnO surface during cyclic processing in precursor solutions followed by removal of excess reagent from the surface of the substrate by washing in hydrogen peroxide. To stabilise the surface states and saturate with oxygen, the surface was annealed in a diffusion furnace. XRD, RAMAN, and SEM analyses were used to analyse the phase composition, structural, and substructural parameters. The nanocomposite film consists of different types of oxides, namely trigonal TeO_3, Monoclinic TeO_4 and $CdTe_3O_8$, orthorhombic TeO_2 and $CdTeO_3$. The formation of films is explained using the Volmer–Weber growth mechanism. SEM analysis of the formed nanocomposite showed the presence of nanometer-scale globules. Partial amorphization of the heterostructure occurs due to the presence of nanometer-sized particles.

Keywords SILAR method · Cadmium-tellurium oxides · Electrolyte · Nanocomposite · Heterostructure

1 Introduction

In recent decades, researchers have focused on the acquisition of thin semiconductor films due to the breadth of their application in various fields of optoelectronic technology [1–7]. Thin films based on materials from the A^2B^6 group deserve special attention due to the possibility of applications in solar energy, lasers and sensors [3, 4, 8, 9]. Thus, cadmium semiconductors, in particular CdTe, CdSe, CdS, etc., are widely used [5, 6, 10, 11]. CdSe is considered promising for the creation of thin film transistors and gamma-ray detectors due to the direct band gap and the ability to adjust resistivity in wide ranges [7, 12]. In addition, studies of CdTe are of great interest, which is rightfully considered a semiconductor of technological importance due to its wide use in solar energy [8, 9, 13–19].

Not less promising and interesting are oxide semiconductors and heterostructures or semiconductors with a layer of their own oxide on the surface [20, 21]. Synthesised arrays of ZnO nanowires demonstrated excellent homogeneity in morphology and geometric characteristics, which may be beneficial for efficient electron transport [22]. At the same time, the main drawback of this material is the wide band gap, which limits the absorption and use of the visible region. To optimise functional properties and increase photocatalytic activity, narrow-band semiconductors such as CdS, CdSe, and CdTe are deposited on the ZnO surface [23, 24]. The problems of growing such structures are primarily related to the high chemical activity of the synthesised films, which leads to a decrease in the photoactivity of the surface. The solution to this problem can be the application of thin layers of oxides, which perfectly protect the surface from photocorrosion [25].

The synthesis of complex cadmium-tellurium oxides, which exhibit the properties of direct-band semiconductors, was reported [26]. On the other hand, such oxides are

✉ Yana Suchikova
yanasuchikova@gmail.com

✉ Anatoli I. Popov
popov@latnet.lv

[1] Berdyansk State Pedagogical University, Berdyansk, Ukraine

[2] L.N. Gumilyov Eurasian National University, 010008 Astana, Kazakhstan

[3] Institute of Solid State Physics, University of Latvia, 8 Kengaraga Street, Riga 1063, Latvia

often present on the surface in the amorphous phase and exhibit the properties of transparent glass [27]. This makes cadmium-tellurium oxides interesting from the point of view of applying them to the surface of heterostructures. In this aspect, the methods of their synthesis, as well as the possibility of controlling the surface and bulk properties of materials by adjusting the O content in the compounds, require research.

Synthesis methods are crucial to ensure the surface morphology, crystallinity, and composition of nanostructures and thin films [28, 29]. $CdTeO_3$ films were grown using reactive pulsed laser deposition [30]. Cadmium oxides with nanobelt-type morphology were prepared using the sol–gel method, which exhibited excellent photocatalytic properties [31].

Conventionally, the methods for the synthesis of thin films can be divided into physical and chemical methods. Physical methods are characterised by the deposition of film material from the target source onto the surface of the substrate [32]. These methods include vacuum evaporation and sputtering, and high temperature and/or pressure regimes are often used [33, 34]. Chemical methods for synthesis of nanocoatings include chemical deposition from the gas phase, laser CVD, organic chemical deposition of metals (MOCVD), chemical and electrochemical etching, etc. [35–37]. In recent years, the technology of a Successive Ionic Layer Adsorption and Reaction (SILAR) has gained popularity, as it allows the deposit of thin films on large areas. This method can be considered a modification of the chemical precipitation method, with the difference that SILAR is implemented by repeating the reaction steps with intermediate sample washing steps. This technology is inexpensive, as it does not require high-tech equipment, a vacuum, and long periods of experimentation [38, 39]. The SILAR method allows for layer-by-layer formation of structural elements of different dimensions with specified properties. The deposition rate and film thickness can easily be controlled by varying the deposition cycles.

In this paper, we report the synthesis of a $Cd_xTe_yO_z$ nanocomposite on the surface of the CdS/ZnO heterostructure by the SILAR method, and we also investigate the morphological, structural, and phase properties of the formed structure.

2 Experiment and materials

CdS samples grown by electrochemical deposition on ZnO monocrystalline plates were used for the experiment. To form the CdS/ZnO structure, the cadmium chloride solution prepared according to the following recipe was used: 0.1 M $CdCl_2$ + 0.1 M CH_4N_2S + 5 M NH_3. The mixture was dissolved in 100 ml of distilled water and stirred with a magnetic stirrer for 20 min at a temperature of 80 °C. The ZnO sample was immersed in the prepared solution and kept for 5 h. After the experiment, the samples were washed in distilled water. It should be noted that the surface of CdS after electrochemical deposition has a large number of broken bonds, which leads to partial oxidation with the formation of CdO cadmium oxide.

The $Cd_xTe_yO_z$ oxides on the CdS/ZnO substrate were formed by the successive ionic layer adsorption and reaction method (SILAR) during cyclic treatment in precursor solutions with subsequent removal of excess reagent from the substrate surface by washing in H_2O_2 (Fig. 1). The number of processing cycles is 5. The use of five processing cycles ensures that sufficient time and reagents are available to precipitate the complex oxide products that form in the chemical reaction between Te and Cd ions. In addition, the number of processing cycles depends on the amount of material required for a thin uniform film evenly distributed over the substrate. Based on our empirical data and literature sources, it was established that a greater or lesser number of processing cycles will lead to the formation of a film that is too thick or too thin, which may be unevenly distributed over the surface [39]. One cycle consisted of four stages:

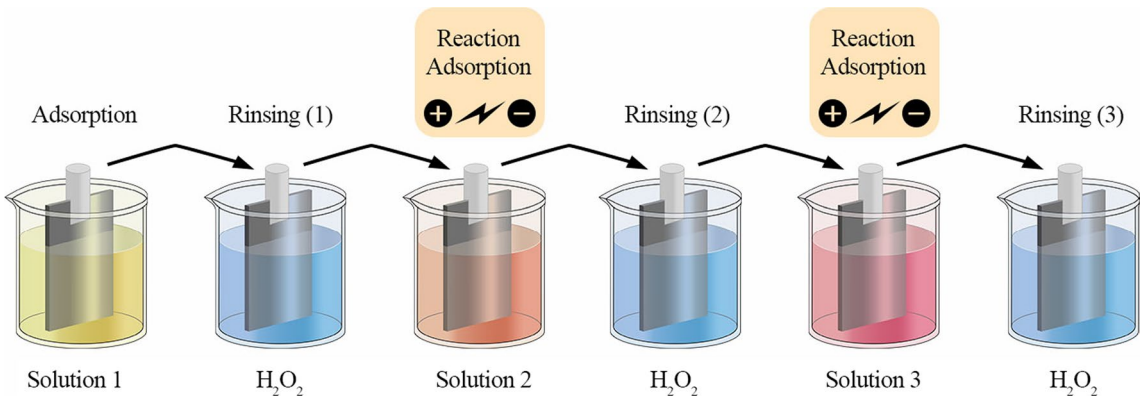

Fig. 1 Schematic illustration of the formation of thin films in the SILAR method

- 1 stage. Immersion of the samples in the precursor—aqueous solution of 0.01 M Na_2TeO_3, processing time—10 min. The solution was heated to 50 °C. During this stage, Te ions are adsorbed on the surface and enter a chemical reaction with the substrate ions.
- 2nd stage. Washing of the samples in H_2O_2 hydrogen peroxide to remove excess tellurium atoms and reaction products. Processing time—2 min.
- 3rd stage. Immersion of the samples in the precursor—alcohol solution of 0.01 M $Cd(NO_3)_2$. The temperature of the solution is 50 °C. During this stage, Cd ions are adsorbed on the surface, and $Cd_xTe_yO_z$ compounds are formed.
- 4th stage. Repeated washing of the samples in H_2O_2 to remove weakly bound ions for 2 min.

For better adsorption and adhesion, electrolytes were stirred with a magnetic stirrer at low speed during deposition. After completing five cycles of processing the samples using the SILAR method, annealing was carried out in a JetFirst diffusion furnace for 20 min at a temperature of 150 °C. The annealing was carried out in atmospheric air to stabilise the surface states due to saturation of the surface with O. This regime was chosen because this temperature is effective in stabilising surface states due to saturation of the O surface and will not allow the evaporation of other elements. Furthermore, on the basis of our own empirical studies, it was established that 20 min is the minimum time required to stabilise the surface states of the $Cd_xTe_yO_z$ nanocomposite. After that, the samples were kept outdoors for 3 months.

The morphology of the films was studied using the SEO-SEM Inspect S50-B microscope at 20 kV. Elemental analysis of the surface was performed using energy dispersive spectrometry. Quantitative evaluation of the spectra was carried out in the self-calibrating detector mode. X-ray diffraction (XRD) and RAMAN spectroscopy were used to analyse the phase composition and structural and substructural parameters.

3 Results and discussion

3.1 XRD analysis

XRD spectra were measured in the angle range of 20–80. This range will be chosen as it corresponds to the typical range of diffraction angles for crystalline materials CdO, TeO_2, TeO_3, TeO_4, $CdTe_3O_8$, $CdTeO_3$, allowing for the identification of the crystal structure and determination of lattice parameters (Fig. 2). The XRD patterns of the $Cd_xTe_yO_z$ films grown by the SILAR method and theoretical patterns CdO, TeO_2, TeO_3, TeO_4, $CdTe_3O_8$, $CdTeO_3$ are shown in Fig. 3. The presence of peaks of binary tellurium oxides (TeO_2, TeO_3, TeO_4) and ternary cadmium-tellurium oxides ($CdTe_3O_8$, $CdTeO_3$) can be observed. The most intense peaks correspond to $CdTe_3O_8$. This indicates the predominance of this oxide over others in the formed nanocomposite.

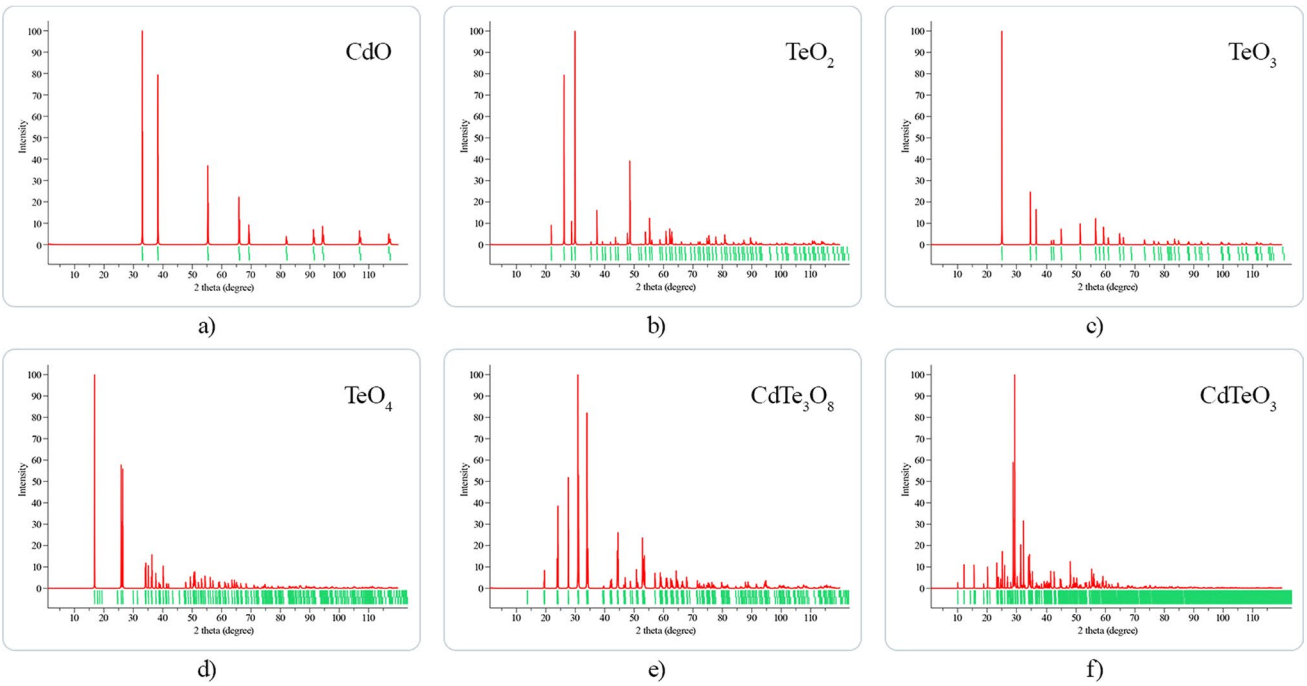

Fig. 2 Theoretical peaks XRD for CdO (**a**), TeO_2 (**b**), TeO_3 (**c**), TeO_4 (**d**), $CdTe_3O_8$ (**e**), $CdTeO_3$ (**f**) (obtained from VESTA)

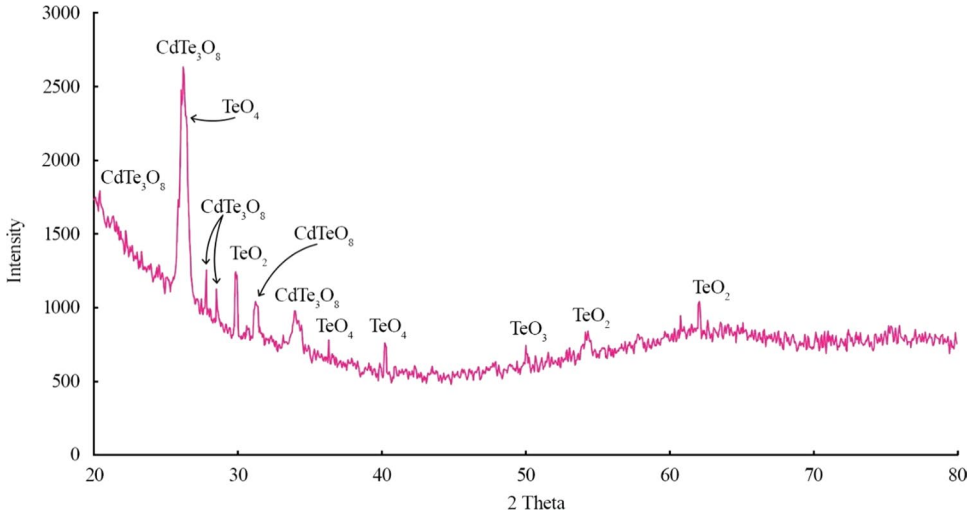

Fig. 3 XRD spectra of nanocomposite $Cd_xTe_yO_z$

Table 1 Crystal structures determined by XRD

No	2θ, °	*hkl*	Oxide	Crystal system
1	50.05	(220)	TeO_3	Trigonal
2	20.1	(111)	$CdTe_3O_8$	Monoclinic
3	26.35	(310)		
4	27.85	(112)		
5	33.95	(020)		
6	26.5	(111)	TeO_4	Monoclinic
7	36.6	(112)		
8	40.34	(020)		
9	31.45	(040)	$CdTeO_3$	Orthorhombic
10	54.4	(220)		
11	63.85	(004)		
12	75.5	(110)		
13	29.95	(102)	TeO_2	Orthorhombic
14	62.05	(024)		

In addition, the intense peak at $2\theta = 26.5°$ is associated with the presence of binary oxide TeO_4 (Fig. 3, Table 1). It can be seen that the oxides $CdTe_3O_8$ and TeO_4 have a similar crystal structure (Fig. 4). It is opinion that TeO_4 is the structural component of $CdTe_3O_8$ [40]. These oxides crystallise on the surface in a monoclinic crystal lattice and have adjacent space group numbers—13 and 14 for $CdTe_3O_8$ and TeO_4, respectively.

Similarly, the similarity of the crystal lattices and parameters of TeO_2 and $CdTeO_3$ (Fig. 5) gives reason to assert the common nature of the formation of these oxides [40, 41]. Their crystal lattices belong to orthorhombic space group numbers, group numbers—61 and 62 for $CdTeO_3$ and TeO_2, respectively. The rather small values of the peak width at half-height indicate that the crystallites are nanometre-sized. On the other hand, the existing noise and low intensity of the peaks of TeO_2, TeO_3, $CdTeO_3$

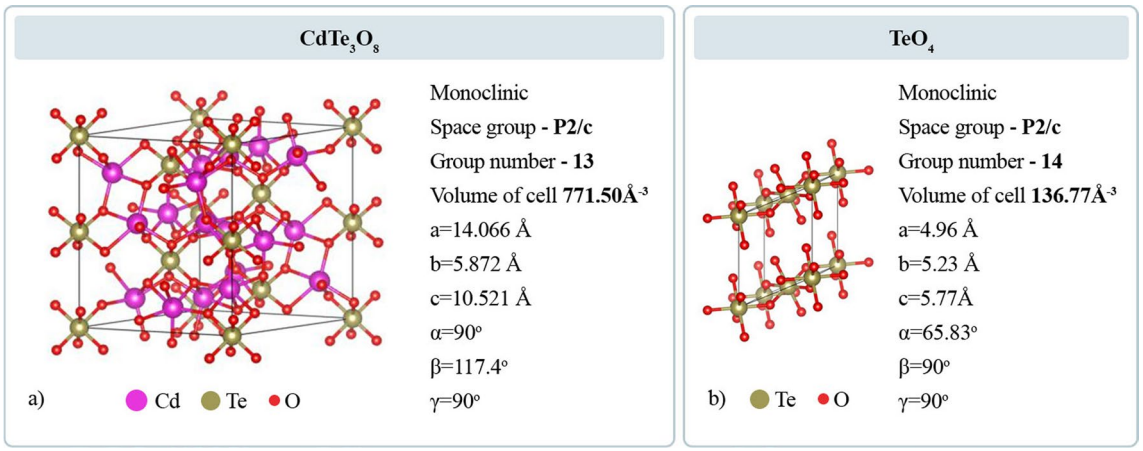

Fig. 4 Crystal lattices and structural parameters of $CdTe_3O_8$ (**a**) and TeO_4 (**b**)

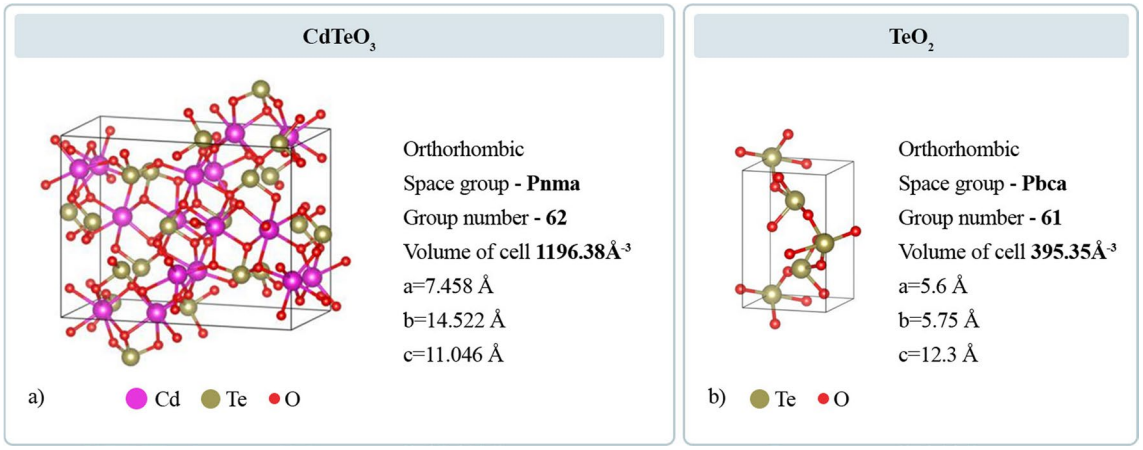

Fig. 5 Crystal lattices and structural parameters of $CdTeO_3$ (**a**) and TeO_2 (**b**)

indicate surface amorphization. That is, these oxides can be on the surface in the form of transparent glass. It should also be noted that most of the peaks compared to the theoretical ones (Figs. 2, 3) show a shift to the left, which may also indicate the formation of oxide layer in the form of nanometre-sized crystallites.

The very weak peak at $2\theta = 50.05°$ corresponds to the trigonal phase TeO_3. Therefore, it is possible to assume that this oxide is formed on the surface of the CdS substrate, the sources of oxygen of which are CdO atoms. Additionally, when O is supplied, TeO_4 is formed by the following reaction:

$$2OH^- + TeO_3^{2-} \rightarrow TeO_4^{2-} + H_2O + 2^{e-}.$$

The following is the attachment of cadmium atoms to the formation of $CdTe_3O_8$. An alternative process is also possible, the eruption of oxygen atoms from TeO_3. In this case, TeO_3 goes to TeO_2. When the surface is saturated with Cd atoms, TeO_2 becomes a source of formation of the ternary oxide $CdTeO_3$. That is, TeO3 is a more energetically favourable form for the formation of tellurium oxides on the surface of CdS covered with CdO nanoparticles. This is explained by a greater correspondence of the TeO_3 parameters of the crystal lattices with CdS and CdO in comparison with other tellurium oxides. With further ionic oxidation of the surface of the sample, there is a transition to other tellurium oxides ($TeO_2 \leftarrow TeO_3 \rightarrow TeO_4$), as described above.

Note that the XRD peaks from CdS, CdTe, and CdO have not been detected. There are several important conclusions from this:

- As a result of the deposition of ion layers on the surface of the heterostructure, CdS/ZNO formed a rather dense nanocompository layer $Cd_xTe_yO_z$;
- Due to the presence of nanometric particles, partial amorphization occurred both on the surface and on the volume of the structure;
- Most likely, CdO on the CdS surface was present in the form of nanoparticles;
- CdTe was not formed on the surface of the CdS/ZnO heterostructure; instead, oxidation processes with the formation of complexes of $Cd_xTe_yO_z$ oxides took place.

A very good match between the crystal lattice parameters of the surface of CdS and CdTe should lead to the formation of CdTe on the surface of CdS by replacing S atoms with Te atoms. However, this did not happen, which once again confirms the presence of a passivating layer of cadmium oxide on the CdS/ZnO surface. Due to its high chemical activity, the SILAR method allows for the processes of dissolution of the passivating layer with the subsequent formation of new oxide compounds. In this way, the crystal lattices of the surface layers are rearranged, and the material acquires new properties.

3.2 Raman spectra analysis

Figure 6 shows the Raman spectrum of the $Cd_xTe_yO_z$ nanocomposite synthesised on the CdS/ZnO surface. Three characteristic regions can be seen. In the low-frequency part of the spectrum, the presence of medium intensity spectra is observed. The most intense peak is at a frequency of 602 cm^{-1}. In the high-frequency part of the spectrum, the presence of low-intensity oscillatory peaks is observed. In this area, the spectrum also shows a sharp rise, which may be due to the heating of the sample during the recording of the spectra.

All combination modes were identified and listed in the Table 2. In general, the main peaks are attributed to tellurium oxides (TeO_2, TeO_3, TeO_4). The most intense peak at

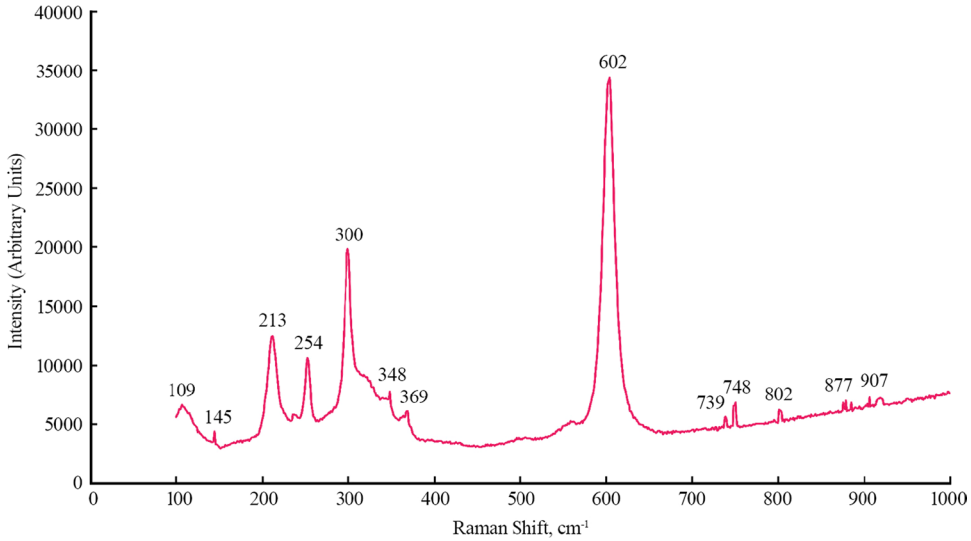

Fig. 6 Raman scattering spectra of the $Cd_xTe_yO_z$ nanocomposite formed on the surface of the CdS/ZnO heterostructure by the SILAR method

Table 2 Band assignment from Raman spectra

ν_c[a], см$^{-1}$	Band	Assignment	References
109 w	A_g	Te–O–Te	[41, 43, 45]
	B_1	Phonon vibrations—Te structure	[44]
145 vw	A_1	Phonon vibrations—Te structure;	[45]
	E	Intra-chain vibrations of Te–Te bonds	[44, 48]
213 m	*E* (LO)	TeO_2	[44, 48]
254 m	TO	β-CdO	[49]
300 s	(B_1+E)	γ-TeO_2	[44, 47]
348 w	*E* (2LO)	TeO_2 asymmetric deformation	[41, 44]
369 w	*D*	TeO_3 asymmetric deformation	[41]
602 vs	*D*	Stretching vibrations TeO_4	[43]
	B_1	Asymmetric stretching vibrations in Te–O–Te bridges as in γ-TeO_2	[44]
739 vw	B_2	Stretching vibrations TeO_3	[44]
		Non-bridging elongation of Te–O (NBO) bonds in TeO_3 polyhedra;	
	E (LO)	α-TeO_2	[47]
		$CdTeO_3$	[48]
748 w	*E* (LO)	α-TeO_2	[42]
		Non-bridging elongation of Te–O (NBO) bonds in TeO_4 polyhedra	[44]
		γ-TeO_2	[47]
750–910 vw	A_1, B_1	γ-TeO_2, TeO_4	[43, 45–47]
	E (TO)	$Cd_xTe_yO_z$	[42, 44, 48]

[a]*vs* very strong, *s* strong, *m* medium, *w* weak, *vw* very weak

602 cm^{-1} is associated with asymmetric stretching vibrations on Te–O–Te bridges, as in γ-TeO_2 (or TeO_4). An intense peak of 300 cm^{-1} is also attributed to crystalline γ-TeO_2. This is consistent with the results of previous studies [41–49], as well as with the results of XRD analysis.

In general, the structure of tellurium oxide TeO_2 consists of TeO_4 trigonal bipyramids, TeO_{3+1} polyhedra, and TeO3 trigonal pyramids. In the TeO_{3+1} structure, the subscript indicates that one O atom is a greater distance from the Te atom than the other three [44]. When this atom is significantly removed, the Te–O bond breaks with the formation of TeO_3 oxide. Such a special configuration of tellurium oxides complicates the interpretation of its spectra. It is often impossible to clearly establish the nature of the peak, which can be interpreted as the contribution of various components of the structure (Table 2) [42–48].

The Raman spectrum clearly demonstrates that during the structural phase transition, TeO_3 transforms into TeO_2, which is compatible with orthorhombic $CdTeO_3$. We can also see that crystalline TeO_4 is compatible with $CdTe_3O_8$.

Thus, when oxygen and tellurium are attached to the surface of the CdS/ZnO heterostructure, we have two phase transitions: hexagonal → cubic → trigonal. Furthermore, upon saturation with Cd and O atoms, the trigonal tellurium oxide TeO_3 transitions to the monoclinic and orthorhombic configuration of the crystal lattice (Fig. 7). These phase transitions depend on the ratio of the Cd–O–Te components in the synthesised $Cd_xTe_yO_z$ nanocomposite. Extreme cases are the formation of Cd_xO_z and Te_yO_z oxides at $x=0$ and $y=0$, respectively (Fig. 7). Excess O content, as well as the formation of Cd–O–Te bonds in $CdTeO_3$ and $CdTe_3O_8$ structures leads to polycrystallisation of the surface and partial amorphization due to the presence of nanometre-sized crystallites. This partly explains the low intensity of the peaks in the Raman light scattering spectra in the range of 700–950 cm^{-1}. It is also consistent with the XRD analysis results presented above.

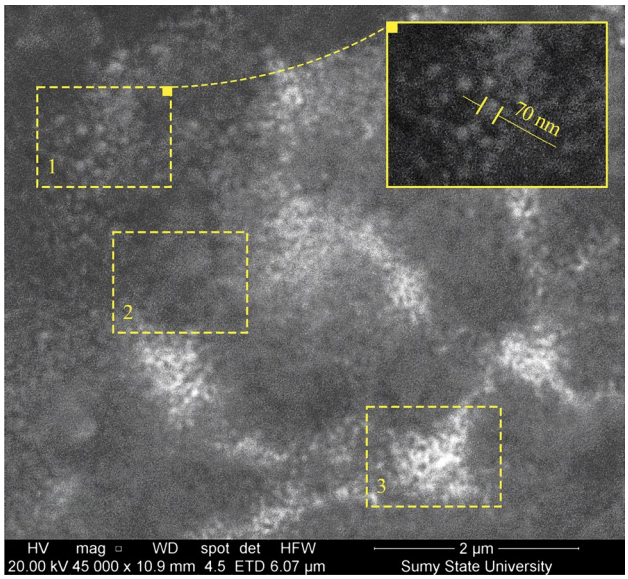

Fig. 8 SEM image of the surface morphology of $Cd_xTe_yO_z$ nanocomposite material synthesised on CdS/ZnO substrate by the SILAR method

3.3 SEM and EDX analyses

During the ion deposition of Cd and Te using the SILAR method on a CdS/ZnO substrate, it was possible to obtain films with densely packed globular structure and a structural element size of the order of 70–90 nm (Fig. 8). It can be seen from the figure that the structure consists of several structural phases. Phase 1 is characterised by the presence of nanometre-sized a large concentration of spherical globules. Phase 2 has a loose "cloud structure". Phase 3—White areas on the morphology image, which are characterised by the presence of a system of branched pores on the surface of the nanocomposite. It can be seen that these areas create a grid over the entire surface; shallow craters consisting of the 1st and 2nd phases are located between the walls of the grid.

EDX analysis taken at three different points of the surface (Fig. 9, Table 3) shows slightly different concentrations of elements on the surface. So, at point 1 (Fig. 9), which corresponds to phase 1 of Fig. 8, you can see the presence of only Cd, Te, and O atoms. O is in a higher concentration, which may indirectly indicate the presence of TeO_4 and $CdTe_3O_8$ oxides in these areas, which is also evidenced by the higher concentration of Te in relation to Cd. Spectrum 2 shows almost stoichiometric content of cadmium and tellurium atoms, as well as a small amount of sulphur. That is, the structure of phase 2 is characterised by a loose porous morphology, through which the CdS substrate "sees through". Interesting results were obtained for spectrum 3. Here, in addition to the main elements (Cd, Te, O), you can see the presence in small concentrations of Zn and S. That is, in these areas (phase 3, Fig. 8) peaks from Zn are very weak

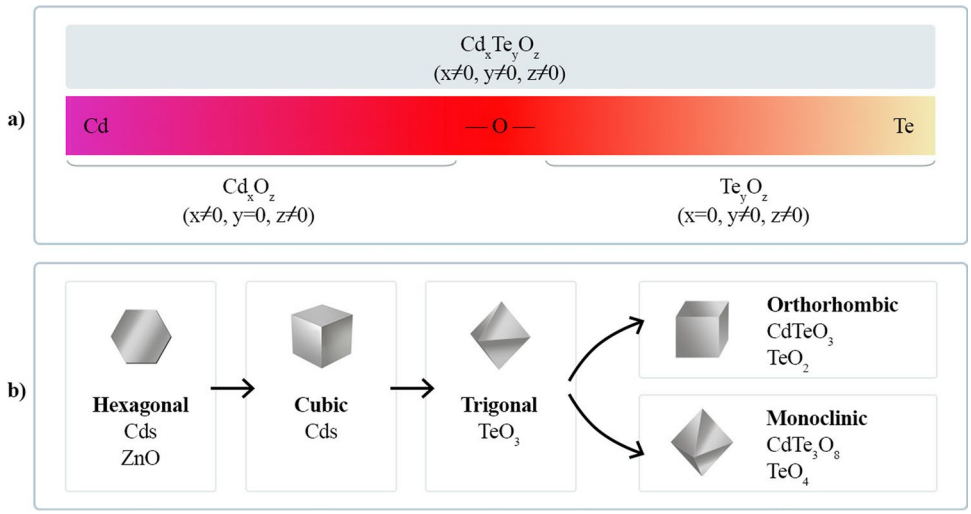

Fig. 7 **a** the ratio of Cd, O, and Te elements in the nanocomposite $Cd_xTe_yO_z$; **b** phase transitions in the $Cd_xTe_yO_z$/CdS/ZnO heterostructure

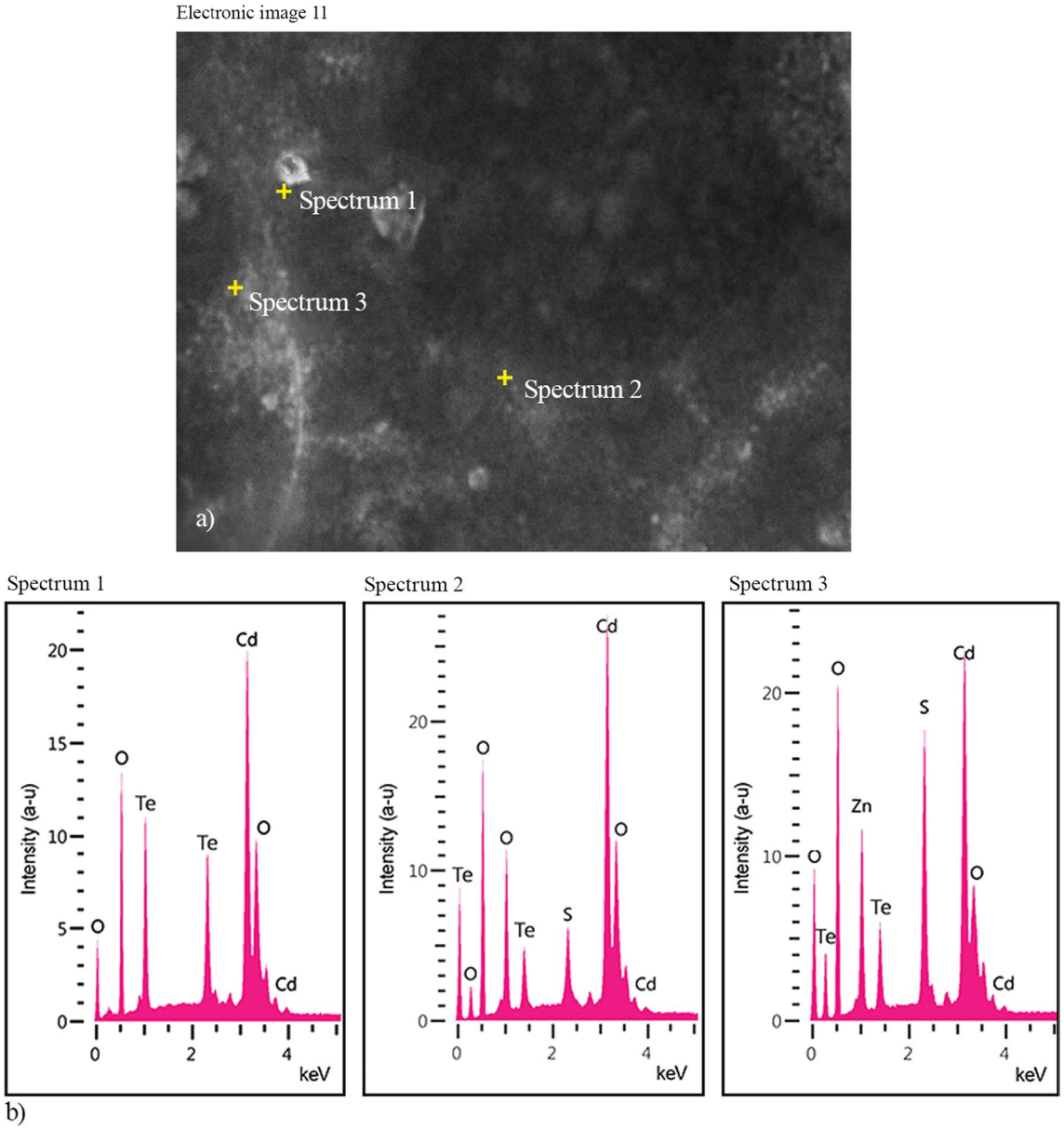

Fig. 9 EDX analysis of the surface of the $Cd_xTe_yO_z$/CdS/ZnO sample: **a** the surface section for which the analysis of the component composition was performed; **b** EDX spectra taken at three points on the surface of the sample

Table 3 Component composition of elements on the surface of the synthesised nanocomposite (atomic units)

Spectrum no	Te, %	O, %	S, %	Zn, %	Cd, %
Spectrum 1	29.49	45.73	0	0	24.78
Spectrum 2	28.76	38.37	5.13	0	27.74
Spectrum 3	21.42	35.52	9.39	3.55	30.12

and appear as a result of "transmission" of a thick layer of ZnO through the structure of CdS, CdO, $Cd_xTe_yO_z$.

From these results, it is possible to predict the growth mechanism of the $Cd_xTe_yO_z$ oxide layer on the CdS/ZnO surface (Fig. 10). As a rule, loose, uneven layers with nanocrystallites separated from each other grow on the surface of the substrate according to the Volmer–Weber mechanism. The Volmer–Weber mechanism is a growth mode in which the film grows by forming isolated islands on the substrate [50]. With further growth, the islands can merge until a continuous film forms. This film growth corresponds to a situation in which Te–O and Cd–O–Te bonds are stronger than those

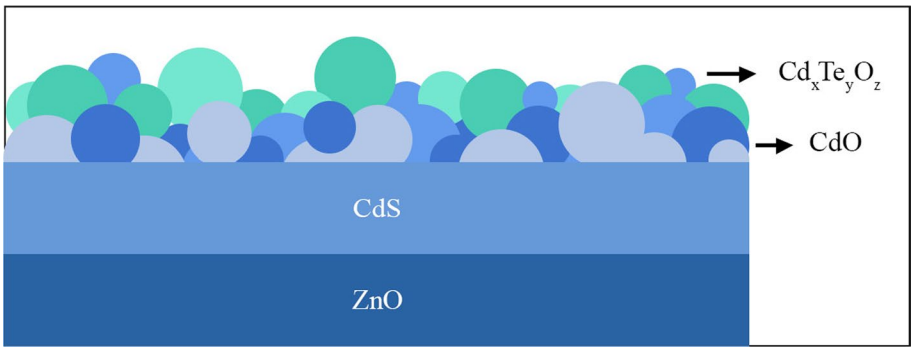

Fig. 10 Schematic representation of the $Cd_xTe_yO_z$/CdS/ZnO nanocomposite

with the substrate. This issue requires further research to improve the synthesis technologies of high-quality $Cd_xTe_yO_z$ oxide passivating films, which already look very promising today because of their chemical stability and transparency.

Thus, for the first time, we demonstrated the production of a complex $Cd_xTe_yO_z$ nanocomposite with a densely packed globular structure of nanometre size by the SILAR method. The feasibility of using a CdS/ZnO substrate was also demonstrated for the first time. However, it should be noted that the $Cd_xTe_yO_z$ nanocomposites obtained on the surface of the CdS/ZnO heterostructure by the SILAR method show heterogeneity in morphology and chemical composition and contain many phases. This indicates that the SILAR method exhibits uncontrollability in our case. However, this method is inexpensive, simple, and allows obtaining structures in large sample areas. Therefore, more research is needed on technology for the synthesis of complex composites using the SILAR method, which will allow the formation of materials with predetermined characteristics. Such studies are necessary, first of all, due to the prospects of using $Cd_xTe_yO_z$ films in the creation of dosimeters, phosphors, sensors, and solar batteries [51–54].

4 Conclusions

In summary, our study reports the successful synthesis of $Cd_xTe_yO_z$ nanocomposite films using the SILAR method on a CdS/ZnO surface. Films were grown by repeating deposition cycles using different compositions of ionic electrolytes. Then, the annealing mode in the oxygen flow was applied to complete the process of oxidation of the surface of the heterostructure. As a result, it was established:

The study of XRD and RAMAN spectra made it possible to establish that binary oxides of tellurium (TeO_2, TeO_3, TeO_4) and ternary cadmium-tellurium oxides ($CdTe_3O_8$, $CdTeO_3$) are present on the surface of the structure. It was established that TeO_3 is present in the trigonal phase, $CdTe_3O_8$ and TeO_4 are in the monoclinic phase, and $CdTeO_3$ and TeO_2 are in the orthorhombic phase. From this, we can conclude that in the first stages of ion deposition, TeO_3 is formed, which is subsequently transformed into TeO_2 (compatible with orthorhombic $CdTeO_3$) and TeO_4 (compatible with $CdTe_3O_8$).

In addition, oxides are present on the surface and in the amorphous phase, which may be caused by the presence of nanometer-sized particles and the imperfection of the synthesis technology. Therefore, further studies are needed to establish optimal conditions for the synthesis of $Cd_xTe_yO_z$.

SEM and EDX analysis also showed the presence of three phases on the surface, namely: (1) densely packed globular structure with the size on structural elements of the order of 70–90 nm; (2) loose "cloud structure"; (3) network system of branched pores on the surface of the nanocomposite. Film growth was assumed to occur according to the Volmer–Weber mechanism, which is characteristic of cases of significant mismatch between the crystal lattices of the substrate and the deposited material. The first priority is the growth of TeO_3 oxide, which, when saturated with oxygen atoms, turns into TeO4 or loses oxygen to form TeO_2. When Cd atoms join TeO_4 and TeO_2, they form the oxides $CdTe_3O_8$ and $CdTe_3O_8$, respectively.

Overall, this study provides information on the growth mechanisms and structural properties of $Cd_xTe_yO_z$ nanocomposite films, which may have potential applications in the fabrication of dosimeters, phosphors, sensors, and solar cells.

Author contributions Conceptualization, YS; methodology, YS, SK, IB and ZTK; software, YS and SK; validation YS and AIP; formal analysis; investigation, YS, VP, and AIP; resources, YS, IB, ZTK and AIP; writing—original draft preparation, YS; writing—review and editing, YS, SK, VP and AIP. All authors have read and agreed to the published version of the manuscript.

Funding This work was supported by the Government of Ukraine (Ministry of Education and Science of Ukraine via project 0122U000129 and 0121U10942). In addition, the research of A.I.P was partly supported by the RADON project (GA 872494) within the H2020-MSCA-RISE-2019 call and COST Action CA20129 "Multiscale Irradiation and Chemistry Driven Processes and Related Technologies" (MultIChem). A.I.P. also thanks to the Institute of Solid-State Physics, University of Latvia. ISSP UL as the Center of Excellence is supported through the Framework Program for European universities,

Union Horizon 2020, H2020-WIDESPREAD-01-2016-2017-TeamingPhase2, under Grant Agreement No. 739508, CAMART2 project.

Data availability Data which are required to supporting finding of this study are present in the article.

Declarations

Conflict of interest The author declares no conflict of interest regarding the publication of this paper.

References

1. H. Wang, Z. Zeng, P. Xu, L. Li, G. Zeng, R. Xiao, Z. Tang, D. Huang, L. Tang, C. Lai et al., Recent progress in covalent organic framework thin films: fabrications, applications and perspectives. Chem. Soc. Rev. **48**, 488 (2019). https://doi.org/10.1039/C8CS00376A
2. R. Swartwout, M.T. Hoerantner, V. Bulović, Scalable deposition methods for large-area production of perovskite thin films. Energy Environ. Mater. **2**(2), 119 (2019). https://doi.org/10.1002/eem2.12043
3. M. Zubkins, R. Kalendarev, J. Gabrusenoks, A. Plaude, A. Zitolo, A. Anspoks, K. Pudzs, K. Vilnis, A. Azens, J. Purans, Changes in structure and conduction type upon addition of Ir to ZnO thin films. Thin Solid Films **636**, 694 (2017). https://doi.org/10.1016/j.tsf.2017.05.049
4. T. Schenk, A. Anspoks, I. Jonane, R. Ignatans, B.S. Johnson, J.L. Jones, M. Tallarida, C. Marini, L. Simonelli, P. Hönicke, Local structural investigation of hafnia-zirconia polymorphs in powders and thin films by X-ray absorption spectroscopy. Acta Mater. **180**, 158 (2019). https://doi.org/10.1016/j.actamat.2019.09.003
5. R. Szczesny, A. Scigala, B. Derkowska-Zielinska, L. Skowronski, C. Cassagne, G. Boudebs, R. Viter, E. Szlyk, Synthesis, optical, and morphological studies of ZnO powders and thin films fabricated by wet chemical methods. Materials **13**, 2559 (2020). https://doi.org/10.3390/ma13112559
6. A. Khodasevich, S. Panarin, K. Terekhov, A. Artsemyeva, H. Dolgiy, V.B. Bondarenko, Fabrication of SERS-active substrates by electrochemical and electroless deposition of metals in macroporous silicon. ECS Trans. **53**, 85 (2013). https://doi.org/10.1149/05311.0085ecst
7. N. Khinevich, H. Bandarenka, S. Zavatski, K. Girel, A. Tamulevičienė, T. Tamulevičius, S. Tamulevičius, Porous silicon—a versatile platform for mass-production of ultrasensitive SERS-active substrates. Microporous Mesoporous Mater. **323**, 111204 (2021). https://doi.org/10.1016/j.micromeso.2021.111204
8. T. Potlog, Thin-film photovoltaic devices based on A2B6 compounds, in *Nanostructures and Thin Films for Multifunctional Applications*, vol. 143 (2016). https://doi.org/10.1007/978-3-319-30198-3_5
9. M. Shur, S. Rumyantsev, R. Gaska, Semiconductor thin films and thin film devices for electrotextiles. Int. J. High Speed Electron. Syst. **12**(02), 371 (2002). https://doi.org/10.1142/S0129156402001320
10. W.W. Yu, L. Qu, A.W. Guo, X, Experimental determination of the extinction coefficient of CdTe, CdSe, and CdS nanocrystals. Chem. Mater. **15**, 2854 (2003). https://doi.org/10.1021/CM034081K
11. M. Hou, Z. Zhou, A. Xu, K. Xiao, J. Li, D.L. Qin, Synthesis of group II–VI semiconductor nanocrystals via phosphine free method and their application in solution processed photovoltaic devices. Nanomaterials **11**(8), 2071 (2021). https://doi.org/10.3390/nano11082071
12. X. Peng, L. Manna, W. Yang, J. Wickham, E. Scher, A. Kadavanich, A.P. Alivisatos, Shape control of CdSe nanocrystals. Nature **404**, 59 (2000). https://doi.org/10.1038/35003535
13. G. Khrypunov, S. Vambol, N. Deyneko, Y. Sychikova, Increasing the efficiency of film solar cells based on cadmium telluride. East. Eur. J. Enterp. Technol. **6**(5(84)), 12 (2016). https://doi.org/10.15587/1729-4061.2016.85617
14. A. Bosio, S. Pasini, N. Romeo, The history of photovoltaics with emphasis on CdTe solar cells and modules. Coatings **10**, 344 (2020). https://doi.org/10.3390/coatings10040344
15. A. Akilbekov, R. Balakhayeva, M. Zdorovets, Z. Baymukhanov, F.F. Komarov, K. Karim, A.I. Popov, A. Dauletbekova, Ion track template technology for fabrication of CdTe and CdO nanocrystals. Nucl. Instrum. Methods Phys. Res. Sect. B **481**, 30 (2020). https://doi.org/10.1016/j.nimb.2020.08.009
16. R. Balakhayeva, A. Akilbekov, Z. Baimukhanov, A. Usseinov, S. Giniyatova, M. Zdorovets, L. Vlasukova, A.I. Popov, A. Dauletbekova, CdTe nanocrystal synthesis in SiO_2/Si ion-track template: the study of electronic and structural properties. Phys. Status Solidi A Appl. Mater. Sci. **218**, 2000231 (2021). https://doi.org/10.1002/pssa.202000231
17. P. Ščajev, A. Mekys, L. Subačius, S. Stanionytė, D. Kuciauskas, K.G. Lynn, S.K. Swain, Impact of dopant-induced band tails on optical spectra, charge carrier transport, and dynamics in single-crystal CdTe. Sci Rep **12**, 12851 (2022). https://doi.org/10.1038/s41598-022-16994-7
18. H.C. Kim, H.G. Jo, The effect of Te-doping and heat treatment on the structural properties of CdTe absorber layer for CdS/CdTe solar cell. Opt. Mater. **134**, 113061 (2022)
19. R. Balakhayeva, A. Akilbekov, Z. Baimukhanov, S. Giniyatova, M. Zdorovets, Y. Gorin, A.I. Popov, A. Dauletbekova, Structure properties of CdTe nanocrystals created in SiO_2/Si ion track templates. Surf. Coat. Technol. **401**, 126269 (2020). https://doi.org/10.1016/j.surfcoat.2020.126269
20. Y.O. Suchikova, I.T. Bogdanov, S.S. Kovachov, Oxide crystals on the surface of porous indium phosphide. Arch. Comput. Mater. Sci. Surf. Eng. **2**(98), 49 (2019). https://doi.org/10.5604/01.3001.0013.4606
21. S.O. Vambol, I.T. Bohdanov, V.V. Vambol, Formation of filamentary structures of oxide on the surface of monocrystalline gallium arsenide. J. Nano Electron. Phys. **9**(6), 060161 (2017). https://doi.org/10.21272/jnep.9(6).06016
22. T.K. Van, L.Q. Pham, D.Y. Kim, Formation of a CdO layer on CdS/ZnO nanorod arrays to enhance their photoelectrochemical performance. Chemsuschem **7**(12), 3505 (2014). https://doi.org/10.1002/cssc.201402365
23. C. Eley, T. Li, F. Liao, S.M. Fairclough, J.M. Smith, G. Smith, Nanojunction-mediated photocatalytic enhancement in heterostructured CdS/ZnO, CdSe/ZnO, and CdTe/ZnO nanocrystals. Angew. Chem. **126**(30), 7972 (2014). https://doi.org/10.1002/ange.201404481
24. T.R. Gurugubelli, R.V. Ravikumar, R. Koutavarapu, Enhanced photocatalytic activity of ZnO–CdS composite nanostructures towards the degradation of rhodamine B under solar light. Catalysts **12**(1), 84 (2022). https://doi.org/10.3390/catal12010084
25. Y. Lai, Y. Wang, Y. Zhu, R. Guo, Y. Xia, W. Huang, Z. Li, Irregular micro-island arrays of CdO/CdS composites derived from electrodeposited Cd for high photoelectrochemical performances. J. Electrochem. Soc. **165**(3), H91 (2018). https://doi.org/10.1149/2.0321803jes
26. R.S. Kapadnis, S.S. Kale, V.G. Wagh, Studies on chemically synthesis of polycrystalline CdTeO3 thin films. Studies **3**(8), 1 (2013)
27. H. Arizpe-Chávez, R. Ramírez-Bon, F.J. Espinoza-Beltrán, O. Zelaya-Angel, J. González-Hernández, L. Baños, Optical and

structural properties of CdTe-$CdTeO_3$ nanocrystalline composites. AIP Conf. Proc. **378**(1), 203 (1996). https://doi.org/10.1063/1.51213
28. Y. Suohikova, S. Vambol, V. Vambol, N. Mozaffari, N. Mozaffari, Justification of the most rational method for the nanostructures synthesis on the semiconductors surface. J. Achiev. Mater. Manuf. Eng. **92**(1–2), 19 (2019). https://doi.org/10.5604/01.3001.0013.3184
29. Y. Suchikova, *Porous Indium Phosphide: Preparation and Properties. Handbook of Nanoelectrochemistry* (Springer, Cham, 2016), pp.283–305. https://doi.org/10.1007/978-3-319-15266-0_28
30. R. Castro-Rodríguez, A. Iribarren, P. Bartolo-Pérez, J.L. Peña, Obtaining of polycrystalline $CdTeO_3$ by reactive pulse laser deposition. Thin Solid Films **484**(1–2), 100 (2005). https://doi.org/10.1016/j.tsf.2005.02.011
31. T. Munawar, M.S. Nadeem, F. Mukhtar, S. Manzoor et al., Enhanced photocatalytic, antibacterial, and electrochemical properties of CdO-based nanostructures by transition metals co-doping. Adv. Powder Technol. **33**(3), 103451 (2022). https://doi.org/10.1016/j.apt.2022.103451
32. O.O. Abegunde, E.T. Akinlabi, O.P. Oladijo, S. Akinlabi, Overview of thin film deposition techniques. AIMS Mater. Sci. **6**(2), 174 (2019). https://doi.org/10.3934/matersci.2019.2.174
33. A. Jilani, M.S. Abdel-Wahab, A.H. Hammad, Advance deposition techniques for thin film and coating. Mod. Technol. Creat. Thin Film Syst. Coat. **2**(3), 137 (2017). https://doi.org/10.5772/65702
34. D. Mahana, A.K. Mauraya, P. Pal, P. Singh, S.K. Muthusamy, Comparative study on surface states and CO gas sensing characteristics of CuO thin films synthesised by vacuum evaporation and sputtering processes. Mater. Res. Bull. **145**, 111567 (2022). https://doi.org/10.1016/j.materresbull.2021.111567
35. J.A. Suchikova, V.V. Kidalov, G.A. Sukach, Preparation of nanoporous n-InP (100) layers by electrochemical etching in HCI solution. Funct. Mater. **17**(1), 131 (2010)
36. R. Homcheunjit, P. Pluengphon, A. Tubtimtae, P. Teesetsopon, Structural, optical, and electrical properties via two simple routes for the synthesis of multi-phase potassium antimony oxide thin films. Phys. B **637**, 413885 (2022). https://doi.org/10.1016/j.physb.2022.413885
37. Y.O. Sychikova, I.T. Bogdanov, S.S. Kovachov, Influence of current density of anodizing on the geometric characteristics of nanostructures synthesized on the surface of semiconductors of A3B5 group and silicon. Funct. Mater. **27**(1), 29 (2019). https://doi.org/10.15407/fm27.01.29
38. H.M. Pathan, C.D. Lokhande, Deposition of metal chalcogenide thin films by successive ionic layer adsorption and reaction (SILAR) method. Bull. Mater. Sci. **27**(2), 85 (2004). https://doi.org/10.1007/BF02708491
39. S.P. Ratnayake, J. Ren, E. Colusso, M. Guglielmi, A. Martucci, E. Della Gaspera, SILAR deposition of metal oxide nanostructured films. Small **17**(49), 2101666 (2021). https://doi.org/10.1002/smll.202101666
40. C. Zhao, X. Zou, S. He, $CdTeO_3$ Deposited Mesoporous NiO photocathode for a Solar Cell. J. Nanomater. **2014**, 372381 (2014). https://doi.org/10.1155/2014/372381
41. F. Caballero-Briones, J.L. Peña, A. Martel, A. Iribarren, O. Calzadilla, S. Jiménez-Sandoval, A. Zapata-Navarro, Structural analysis of Cd–Te–O films prepared by RF reactive sputtering. J. Non Cryst. Solids. **354**(31), 3756 (2008). https://doi.org/10.1016/j.jnoncrysol.2008.03.042
42. J. Carmona-Rodríguez, R. Lozada-Morales, O. Jiménez-Sandoval, F. Rodríguez-Melgarejo, M. Meléndez-Lira, S.J. Jiménez-Sandoval, CdTeO*x* to $CdTeO_3$ structural phase transition in as-grown polycrystalline films by reactive sputtering. J. Appl. Phys. **103**(12), 123516 (2008). https://doi.org/10.1063/1.2939567
43. F. Caballero-Briones, A. Zapata-Navarro, A. Martel, A. Iribarren, J.L. Peña, Compositional mixture in RF sputtered CdTe oxide films. Raman spectroscopy results. Superf. Vacio **16**(3), 38 (2003)
44. A. Jayaraman, G.A. Kourouklis, A high pressure Raman study of TeO_2 to 30 GPa and pressure-induced phase changes. Pramana **36**(2), 133 (1991). https://doi.org/10.1007/BF02845698
45. M. Ceriotti, F. Pietrucci, M. Bernasconi, Ab initio study of the vibrational properties of crystalline TeO_2: The α, β, and γ phases. Phys. Rev. B **73**(10), 104304 (2006). https://doi.org/10.1103/PhysRevB.73.104304
46. A. Chagraoui, I. Yakine, A. Tairi, A. Moussaoui, M. Talbi, M. Naji, Glasses formation, characterization, and crystal-structure determination in the Bi_2O_3–Sb_2O_3–TeO_2 system prepared in an air. J. Mater. Sci. **46**(16), 5439 (2011). https://doi.org/10.1007/s10853-011-5485-9
47. İ Kabalcı, G. Özen, M.L. Öveçoğlu, Microstructure and crystallization properties of TeO_2-PbF_2 glasses. J. Raman Spectrosc. **40**(3), 272 (2009). https://doi.org/10.1002/jrs.2119
48. A. Guillén-Cervantes, M. Becerril-Silva, H.E. Silva-López, J.S. Arias-Cerón, E. Campos-González, M. Pérez-González, O. Zelaya-Ángel, Structural and optical properties of CdTe + CdTeO3 nanocomposite films with broad blueish photoluminescence. J. Mater. Sci. Mater. Electron. **31**(9), 7133 (2020). https://doi.org/10.1007/s10854-020-03284-z
49. V. Srihari, V. Sridharan, T.R. Ravindran, S. Chandra, A.K. Arora, V.S. Sastry, C.S. Sundar, Raman scattering of cadmium oxide: in B1 phase. AIP Conf. Proc. **1349**, 845 (2011). https://doi.org/10.1063/1.3606122
50. Z.Y. Hang, C.V. Thompson, Grain growth and complex stress evolution during Volmer–Weber growth of polycrystalline thin films. Acta Mater. **67**, 189 (2014). https://doi.org/10.1016/j.actamat.2013.12.031
51. K. Oh, M. Han, K. Kim, Y. Heo, C. Moon, S. Park, S. Nam, Development and evaluation of cadmium telluride dosimeters for accurate quality assurance in radiation therapy. J. Inst. **11**, C02040–C02048 (2016). https://doi.org/10.11113/mjfas.v5n1.283
52. R. Hussin, N.S. Leong, N.S. Alias, Structural investigation of crystalline host phosphor cadmium tellurite systems. J. Fund. Sci. **5**, 17–27 (2009). https://doi.org/10.1088/1748-0221/11/02/C02040
53. Y.J. Chen, X.P. Yan, Chemical redox modulation of the surface chemistry of CdTe quantum dots for probing ascorbic acid in biological fluids. Small **5**, 2012–2018 (2009). https://doi.org/10.1002/smll.200900291
54. C. Zhao, X. Zou, S. He, $CdTeO_3$ deposited mesoporous NiO photocathode for a solar cell. J. Nanomater. (2014). https://doi.org/10.1155/2014/372381